Test of ^{45}Sc level densities with proton resonances

S. J. Lokitz* and G. E. Mitchell†
North Carolina State University, Raleigh, North Carolina 27695, USA and Triangle Universities Nuclear Laboratory, Durham, North Carolina 27708, USA

J. F. Shriner, Jr.‡
Tennessee Technological University, Cookeville, Tennessee 38505, USA
(Received 23 March 2005; published 23 June 2005)

A high resolution measurement of the cross sections of the ^{44}Ca(p,p_0) and ^{44}Ca(p,p_1) reactions was performed over the energy range $E_p = 2.50$–3.53 MeV. A total of 809 resonances were observed. The purity and completeness of the ^{45}Sc data were tested with a variety of statistical analyses. These analyses suggest that the $1/2^+$ and $1/2^-$ resonance sequences are the most pure and complete ever measured. The resulting level densities are $\rho(1/2)^+ = 127^{+7}_{-8}$ MeV^{-1} and $\rho(1/2^-) = 132^{+8}_{-9}$ MeV^{-1}; there is no evidence of parity dependence of the level density of $J = 1/2$ states at $E_x = 10$ MeV in ^{45}Sc.

DOI: 10.1103/PhysRevC.71.064315 PACS number(s): 21.10.Ma, 24.30.−v, 25.40.Cm

I. INTRODUCTION

Level densities play a central role in many parts of pure and applied nuclear physics. These range from nuclear astrophysics to radiochemical applications for stewardship science. Measurements utilizing proposed new facilities such as the Rare Isotope Accelerator will require predictions of reaction rates far from the stability line, and therefore reliable predictions of level densities will be very important.

Most conventional calculations of the nuclear level density are modifications and extensions of the Fermi gas model. Pairing and shell effects are added semiempirically; see, e.g., Refs. [1–3]. This approach works fairly well in practice, in the sense that one can interpolate with some confidence. However, extrapolating to conditions far from the stability line with semiempirical models seems very questionable. Improved understanding may be provided by new approaches such as the shell model Monte Carlo (SMMC) method [4], which permits the reliable determination of average quantities such as level densities in very large model spaces. For example, Nakada and Alhassid [5,6] have applied this approach to level densities in the iron region.

It would be valuable to have data to test detailed predictions of the level density models. For such key properties as the J dependence or the parity dependence, there is little direct and statistically significant evidence, although a recent study [7] summarizes what is known for low-energy states. The classic approach of using neutron resonances to determine level densities works very well for s-wave resonances, but many p-wave resonances are missed and there is usually ambiguity in the J-value assignments. The situation is much worse for even higher values of orbital angular momentum. The situation is better for proton resonances (the difference in penetrability for different orbital angular momenta is smaller for few MeV proton resonances than for standard neutron resonance experiments). However, although one can see and identify d- and f-wave proton resonances, the fraction of missing levels increases very rapidly with the ℓ value, and identification of J may be even more difficult than for lower ℓ values. In practice, even the proton resonances provide only limited information concerning the J dependence of the level density.

The situation is somewhat better for the parity dependence. In the simplest statistical models, the level densities for the two parities are assumed equal, while SMMC calculations predict a significant parity dependence for some nuclei [5,6]. Since detailed spectroscopic information is required to measure the parity dependence, this rules out methods that determine only the average level density. The requirement of reasonable statistics effectively rules out level densities determined from low-lying states; the number of states with known quantum numbers is almost always too small. This leaves nuclear resonances. As noted above, the classic method of determining nuclear level densities via the counting of neutron resonances is very successful for s-wave resonances, but there are major difficulties with the observation of the p-wave resonances and even more difficulty in determining their J values. In practice, there is extremely little neutron data of sufficient quality to address the parity-dependence question.

Proton resonances appear to present the best opportunity to determine the parity dependence of level densities. Since the difference in s- and p-wave penetrabilities is much smaller for the proton case, the probability of observing p-wave resonances is much larger for protons than for neutrons. For nucleons incident on spin-zero targets, the s-wave resonances have unique spin and parity $1/2^+$, while the p-wave resonances have $J^\pi = 1/2^-$ or $3/2^-$. Our method normally provides a unique assignment for the ℓ value and thus the parity. The major problem for the proton resonance case is determining the J value for the resonances with $\ell > 0$.

*Current address: Duke University Medical Center Durham, NC 27708-3949, USA; Electronic address: stephen.lokitz@duke.edu
†Electronic address: mitchell@tunl.duke.edu
‡Electronic address: jshriner@tntech.edu

Recently [8] we examined several sets of proton resonance data (for ^{44}Ca, ^{48}Ti, and ^{56}Fe targets) obtained by our group and concluded that available data for ^{45}Sc showed a difference in the level densities for $1/2^-$ and $1/2^+$ states that was statistically significant at the 3σ level. In addition to the $p + {}^{44}$Ca data that we analyzed, our group had performed several earlier experiments on ^{44}Ca. Including these data would increase the size of the data set significantly, but at the cost of combining data from experiments performed at different times under different experimental conditions. We decided to remeasure the reaction and to confront the issue of parity dependence with one unified data set obtained under improved experimental conditions.

We have measured the ^{44}Ca(p,p_0) and ^{44}Ca(p,p_1) reactions in the energy range $E_p = 2.50$–3.53 MeV and observed and analyzed approximately 800 resonances [9]. A brief summary of the key results for the $1/2^+$ and $1/2^-$ level densities has been published [10].

The experimental method is briefly reviewed in Sec. II. The analysis procedure used to determine the resonance parameters is presented in Sec. III. Evaluation of the data, including various statistical tests, is given in Sec. IV. The level densities and strength functions are presented in Sec. V. The final section provides a brief summary and conclusions.

II. EXPERIMENTAL METHOD

The experiment was performed at the High Resolution Laboratory of the Triangle Universities Nuclear Laboratory. The high resolution system [11] provided proton beams in the range $E_p = 1$–4 MeV, with beam energy resolution of 250–350 eV. For this experiment, the energy range was $E_p = 2.50$–3.53 MeV with an overall beam energy resolution of about 300 eV. The beam energy calibration was performed with a secondary standard resonance [the $3/2^+$ resonance at $E_p = 3.2369$ MeV in the ^{56}Fe(p,p_0) reaction] determined with respect to a standard neutron threshold [the ^{13}C(p,n) threshold]. Without changing any of the experimental conditions, a d-wave resonance in ^{44}Ca(p,p_0) was located at $E_p = 3.2363$ MeV. This established the energy calibration for the calcium experiment. The calibration provides energies accurate to ± 300 eV near the calibration point and to ± 2 keV away from the calibration point.

The calcium was in the form of $CaCO_3$ enriched to 95.9% ^{44}Ca. The calcium carbonate was reduced with tantalum and then evaporated onto thin carbon backings. Target thicknesses ranged from 1.1 to 1.5 μg/cm^2, which corresponds to approximately 70–120 eV average proton energy loss. Data were obtained for the (p,p_0) and (p,p_1) reactions at laboratory angles of 90°, 108°, 135°, 150°, and 165°. The solid angles were chosen to yield approximately equal count rates in each detector. The detectors were passivated implanted planar silicon (PIPS) detectors with 50 mm^2 active area and 300 micron depth. These detectors had much better energy resolution than the silicon surface barrier detectors used in earlier experiments, a fact that would be important in the resonance analysis. The energy step size was normally 100 eV. Sufficient counts were obtained to provide $\approx 1\%$ statistics for the elastic scattering reaction.

The earlier data [12–15] were obtained under a variety of different experimental conditions. A number of technical improvements have been made since those earlier measurements. An automated data collection system [11] improved the uniformity and overall quality of the data. The overall beam energy resolution was improved relative to the earlier experiments, primarily due to a change in the frequency used in the rf ion source in the accelerator. The improved resolution of the PIPS detectors enabled us to observe and analyze even very weak resonances in the inelastic channel. This proved valuable in determining the J value of p-wave resonances, which in turn was crucial to addressing the parity-dependence question. A much improved computing system was also very important for the data analysis, since this data set had the largest number of resonances that our group has ever attempted to analyze. However, the fact that the results reported here represent measurements with identical equipment, experimental procedures, and analysis procedures is probably as important as the technical improvements are in achieving significantly improved results for this reaction.

III. DATA AND DETERMINATION OF RESONANCE PARAMETERS

The experimental excitation functions were fitted with the multilevel, multichannel R-matrix program MULTI6 [16]. This program, which has been modified extensively over the years by our group, uses the formalism of Lane and Thomas [17]. For a given set of resonance parameters (resonance energy, spin, parity, and all allowed width amplitudes), the program generates excitation functions. These parameters are varied to obtain the best visual fit. The data at all angles and for all reaction channels are fitted simultaneously.

For zero-spin targets such as ^{44}Ca, the orbital angular momentum is usually apparent by examining the elastic scattering cross section. Interference between the Coulomb and nuclear resonance amplitudes leads to a very strong change of resonance shape with angle; except for very weak resonances, the ℓ value is easy to determine by inspection. For orbital angular momentum ℓ, the J value is limited to $\ell \pm 1/2$ for $\ell \geqslant 1$, while of course $\ell = 0$ uniquely identifies the J value as 1/2. The difference between $1/2^-$ and $3/2^-$ resonances is greatest at particular angles; and for strong resonances, the J value is relatively easy to determine solely from the elastic scattering differential cross sections. However, for weak resonances, it is often difficult to determine the spin from elastic scattering data alone. [For pure elastic scattering, the energy integrated cross section depends on the product $(2J+1)\Gamma_p$ and not on Γ_p and J separately.] The problem is accentuated when the level density is large and the resonances are no longer well isolated, as in the present data. For higher ℓ values, the situation tends to be even worse. We observe many d-wave resonances, but the spin determination for these resonances is very difficult. We also observe a significant number of f-wave resonances, but a definitive spin assignment for these resonances is rarely possible.

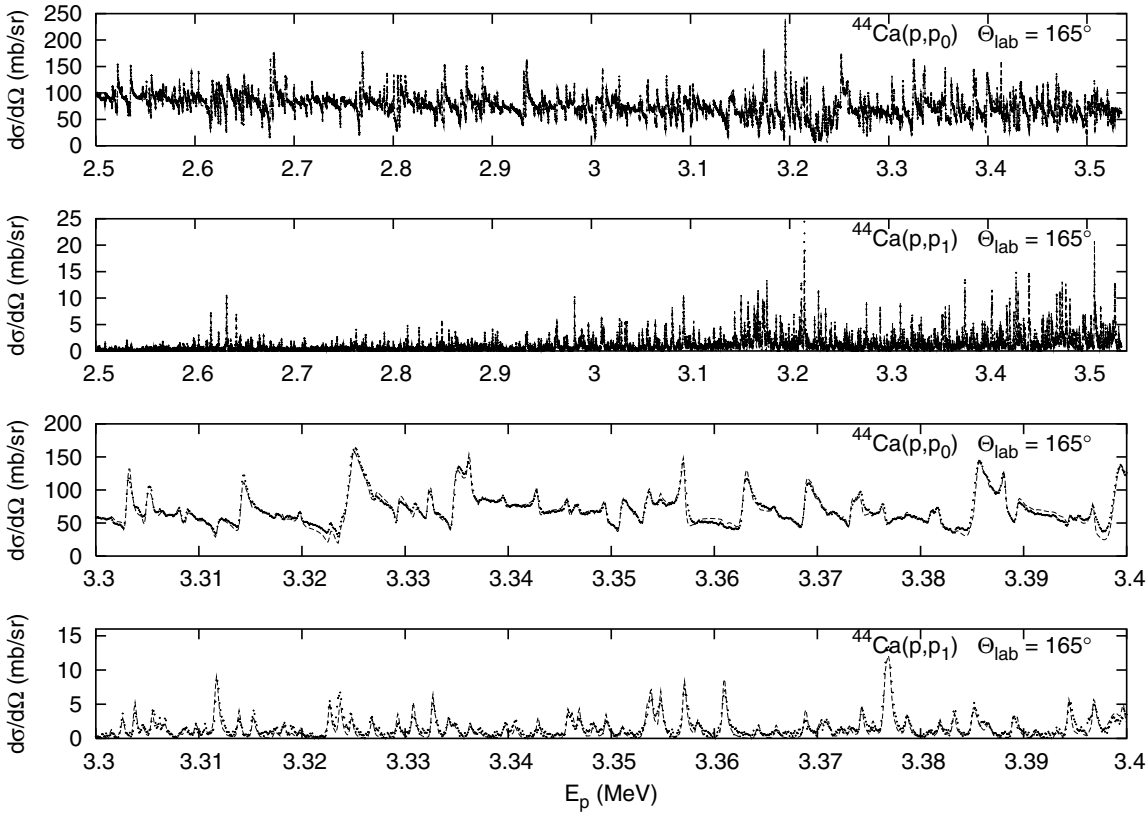

FIG. 1. Data and fits at 165° for the ^{44}Ca(p, p_0) and ^{44}Ca(p, p_1) reactions. The upper figures show the complete energy range studied in these experiments, while the lower figures show a more detailed view of the range $E_p = 3.3$–3.4 MeV.

In this new experiment, we observed 809 resonances, approximately 150 more than observed in the combined data set of the several earlier experiments [12–15]. The data and the corresponding fits for both reactions at 165°, along with a more detailed look at the same information in the range $E_p = 3.3$–3.4 MeV, are shown in Fig. 1.

Table I compares the number of resonances observed in these measurements for each J^π value with the numbers of resonances previously assigned in this same energy range. A complete listing of the resonance parameters is available [18].

The increase in the number of resonances is due in part to the automated data system and to the improved beam resolution, but the most striking improvement is for the inelastic scattering data. With the improved energy resolution in the PIPS detectors, we were able to observe even very weak resonances (total widths of a few eV) and to determine approximate angular distributions. The angular distributions were crucial in the determination of the J value of the p-wave resonances. An anisotropic angular distribution for inelastic scattering from an isolated p-wave resonance means that the state *must* have $J = 3/2^-$. The converse is not true: an isotropic angular distribution does not ensure that the state has $J = 1/2^-$, but this is the most likely spin assignment in that situation. Therefore, the spin assignments for the $\ell = 1$ resonances are believed to be fairly reliable. Sample angular distributions for a $1/2^-$ and a $3/2^-$ resonance are shown in Fig. 2 to illustrate this point.

The inelastic scattering for those resonances with $\ell > 1$ is not as helpful, and the spin assignments are less certain.

We performed statistical tests on all of the level sequences (defined as levels with the same spin and parity). However, even with our improved experimental system and analysis method, the sequences are pure only for the $1/2^+$, $1/2^-$, and $3/2^-$ states. For pure sequences, we can apply missing

TABLE I. Numbers of resonances by J^π assignments in this work and in previous work [12–15] in this same energy range. Definitive spin assignments were not made for $\ell = 3$ and $\ell = 4$ resonances.

	Resonance J^π							
	$\frac{1}{2}^+$	$\frac{1}{2}^-$	$\frac{3}{2}^-$	$\frac{3}{2}^+$	$\frac{5}{2}^+$	$\left(\frac{5}{2}, \frac{7}{2}\right)^-$	$\left(\frac{7}{2}, \frac{9}{2}\right)^+$	Total
Previous work	129	138	125	121	141	0	0	654
Present work	121	116	178	203	117	72	2	809

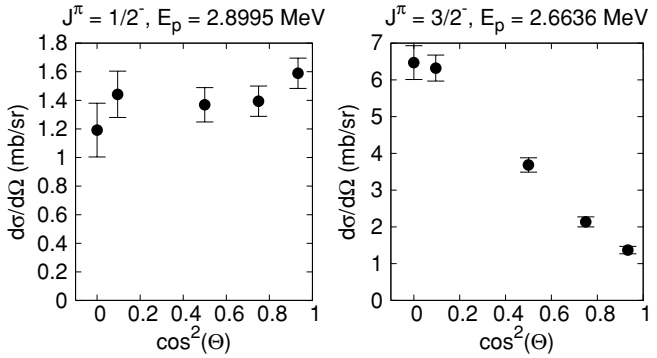

FIG. 2. Angular distributions for the ^{44}Ca(p, p_1) reaction for two p-wave resonances. When plotted in this fashion, isolated $1/2^-$ resonances must have an isotropic distribution for this reaction, while isolated $3/2^-$ resonances are expected to show linear behavior with a slope that is almost always nonzero.

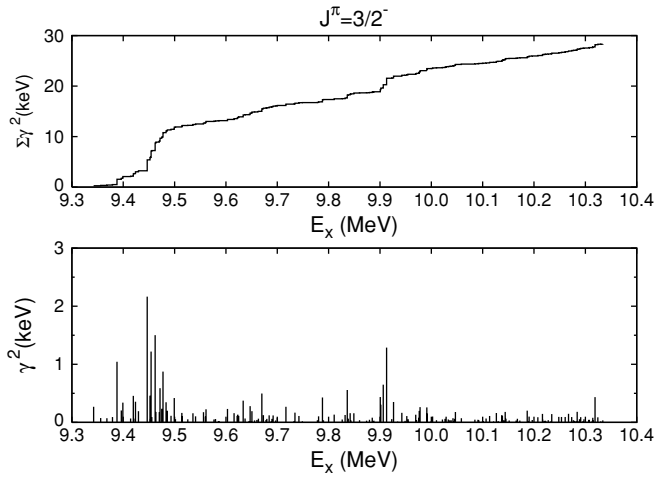

FIG. 3. Reduced widths and sum of reduced widths as a function of excitation energy for the $3/2^-$ states in $p + {}^{44}$Ca.

level corrections with confidence. Since we are interested in the parity dependence of the level density, we focus on the $J = 1/2$ resonances. In the following section, we present evidence to support our claim that the $J = 1/2$ sequences are pure and then discuss the missing level corrections.

IV. DATA EVALUATION

A. Isobaric analog resonances

Isobaric analog resonances must be identified and removed before statistical analyses of the widths are performed. Since an analog resonance is a nonstatistical effect, the "additional" width will distort the reduced width distribution (and therefore the missing level correction) and overestimate the proton strength function. The analog state essentially affects only the widths, leaving the spacings unaffected. This latter issue is considered explicitly in a recent paper [19] and is crucial to the missing level corrections discussed below.

Analog states that occur in the $p + {}^{44}$Ca reactions at a few MeV correspond to low-lying levels in the parent system ^{45}Ca. Since $A = 45$ is in the nuclear $1f$-$2p$ shell, the analogs are expected to have $\ell = 1$ or $\ell = 3$. The analogs are often apparent by inspection of the plots of the reduced widths γ^2 vs energy and the cumulative sums of reduced widths $\Sigma\gamma^2$ vs energy. Strengths of the low-lying parent states are normally much larger than the compound nuclear states, and the result is typically a clear enhancement of the reduced widths, often with a fine structure distribution. Three analogs were identified in earlier studies; all have $\ell = 1$. Examination of six sequences in the present data clearly suggests three fragmented analogs. Of course, there may be other weaker analogs, but the spectroscopic information in the parent nucleus ^{45}Ca [20] is insufficient to identify any additional analogs. The inclusion of additional weak analogs should not have a significant impact on our analyses. However, these three strong analogs would have a major impact if they were not identified and considered. For each of these three states, we identified the lowest-energy and highest-energy fragments of the analog by examination of the reduced widths; those states and all other states of that spin/parity between them in energy were considered part of the analog state and were not included in statistical analyses that involved reduced widths.

The reduced widths and sum of reduced widths for $J^\pi = 3/2^-$ states are shown in Fig. 3. In the lower energy region previously studied by Wilson *et al.* [12], there is a highly fragmented $3/2^-$ analog state near $E_x = 9.4$ MeV, the daughter of the $E_x = 2.842$ MeV state in ^{45}Ca. A total of 19 resonances were identified as belonging to this analog state. Another group of seven $3/2^-$ resonances near E_x 9.91 MeV is identified as the analog of the state in ^{45}Ca at $E_x = 3.241$ MeV. A strong $1/2^-$ resonance at $E_p = 3.002$ MeV had been previously identified [15] as the analog of this state when this state was believed to have $J^\pi = 1/2^-$. However, this state in ^{45}Ca has since been reassigned $J^\pi = 3/2^-$, and the new analog identification reflects that change.

The third analog state identified in this work is near $E_x = 10.0$ MeV; a total of 20 $J^\pi = 1/2^-$ resonances were identified as fragments of this analog. This analog is tentatively identified as the daughter of the $J^\pi = 1/2^-$ state at $E_x = 3.418$ MeV in ^{45}Ca, although it could instead be the daughter of the $E_x = 3.442$ MeV state currently assigned $(1/2, 3/2)^-$. These results are summarized in Table II. In practice these analog states are important, since for both the $1/2^-$ and $3/2^-$ states, the analog strength removed was approximately one-half of the total strength observed for these sequences.

B. Background for statistical tests

Prior to performing any statistical tests, the nuclear level density must be unfolded in order to make the average level spacing constant. The unfolding procedure was described in detail by Shriner *et al.* [21]. For convenience, we employ the simple constant temperature form for the level density. The integrated level density

$$N_{\text{theo}}(E) = \int_0^E \rho(E)dE = e^{(E-E_0)/T} - e^{-E_0/T} + N_0 \quad (1)$$

TABLE II. Summary of analog states identified in ^{45}Sc.

Parent state E_x (MeV)	J^π	Analog fragments E_x (MeV)	Resonance energies E_p (MeV)	Number of fragments	$\sum \Gamma_p$ (keV)	$\sum \gamma_p^2$ (keV)
2.842	$3/2^-$	9.387–9.477	2.5559–2.6476	19	1.66	10.28
3.241	$3/2^-$	9.900–9.925	3.0805–3.1068	7	1.28	3.65
3.442	$1/2^-$	9.956–10.063	3.1383–3.2476	20	19.88	48.22

is compared with the experimental $N(E)$. The best fit $F(E)$ to $N(E)$ is obtained, and a corrected sequence of energies is generated:

$$E_{\rm corr} - E_{\rm min} + (E_{\rm max} - E_{\rm min})\frac{F(E) - F(E_{\rm min})}{F(E_{\rm max}) - F(E_{\rm min})}. \quad (2)$$

The parameter T is related only to the empirical fit and is specific for each sequence. The unfolded level sequences are evaluated with various statistical tests. We consider the nearest-neighbor spacing distribution, the Δ_3 statistic, and the reduced width distribution.

The nearest-neighbor spacing distribution emphasizes the effects of short-range correlations (level repulsion) for the eigenvalues. For a set of spacings S_i, it is convenient to define dimensionless variables

$$x_i = \frac{S_i}{D}, \quad (3)$$

where D is the average spacing. A system that follows the Gaussian orthogonal ensemble (GOE) version of random matrix theory (RMT) has a probability distribution that agrees very nearly with the Wigner distribution [22]:

$$P_{\rm Wigner}(x) = \frac{\pi}{2} x e^{-\pi x^2/4}. \quad (4)$$

This distribution exhibits level repulsion since $P_{\rm Wigner} = 0$ for $x = 0$. On the other hand, a set of uncorrelated levels is expected to have distribution that obeys Poisson statistics:

$$P_{\rm Poisson}(x) = e^{-x}. \quad (5)$$

We also utilize the probability distribution functions $F(x)$ for these two distributions:

$$F(x) = \int_0^x P(x')\,dx', \quad (6)$$

$$F_{\rm Wigner}(x) = 1 - e^{-\pi x^2/4}, \quad (7)$$

$$F_{\rm Poisson}(x) = 1 - e^{-x}. \quad (8)$$

The Δ_3 statistic [23] emphasizes long-range correlations in the eigenvalues. For a series of levels in the energy range $E_{\rm min}$ to $E_{\rm max}$, it is defined as

$$\Delta_3(L) = \min_{A,B} \frac{1}{E_{\rm max} - E_{\rm min}} \int_{E_{\rm min}}^{E_{\rm max}} [N(E) - AE - B]^2 dE. \quad (9)$$

The Δ_3 statistic is a measure of the deviation of $N(E)$ from the best straight-line fit. For Poisson statistics, the expected value of Δ_3 is $L/15$. For GOE statistics, the expected value must be evaluated numerically, but for large L approaches,

$$\Delta_{3_{\rm GOE}}(L) \approx \frac{1}{\pi^2}[\ln L - 0.0687]. \quad (10)$$

The distribution of reduced widths is expected to follow a Porter-Thomas distribution [24]:

$$P(y) = \frac{1}{\sqrt{2\pi y}} e^{-y/2}, \quad (11)$$

where $y = \gamma^2/\langle\gamma^2\rangle$ is a normalized reduced width.

C. Missing and misassigned levels

Missing and misassigned levels can seriously affect each of the statistics discussed above. The issue of spin misassignment does not arise for the $1/2^+$ resonances, but it is a serious consideration for the p-wave resonances. Assuming that random matrix theory applies to these resonance data, the spacing distribution is described by Eq. (4). One can use the properties of this distribution to determine the quality of the experimental data. For example, both large and small spacings are very unlikely; the probabilities of $x \geqslant 3$ and of $x \leqslant 0.04$ are both $\approx$0.001 for this distribution. Sufficiently large values of x therefore suggest that a level was missed, while sufficiently small values of x suggest that a spurious level has mistakenly been assigned to the sequence of levels being considered. When focusing on misassignments, it is convenient to consider the quantity $1/x$. The values of x and $1/x$ for each pair of levels identified as $J^\pi = 1/2^-$ in previous work [12–15] are shown in Fig. 4; the "level index" simply counts successive nearest-neighbor spacings. These data suggest that a significant number of these resonances had an incorrectly assigned spin value.

The results for the $p_{1/2}$ resonances following the recent experimental measurements are shown in Fig. 5. The improvement is quite noticeable, and we conclude that the new $p_{1/2}$ data set appears to have relatively few missing or misassigned levels.

D. General statistical tests

The statistical properties of all of the sequences were evaluated with the three tests described above. The results for the spacing distribution for the $1/2^+$ and $1/2^-$ resonances are shown in Fig. 6. The spacing distribution for the s-wave levels agrees rather well with the Wigner surmise. The spacing distribution for p-wave levels agrees less well, and the spacing distributions for the other sequences do not agree well with the Wigner distribution. This is not surprising: the s-wave resonances are the strongest because of the larger penetrability,

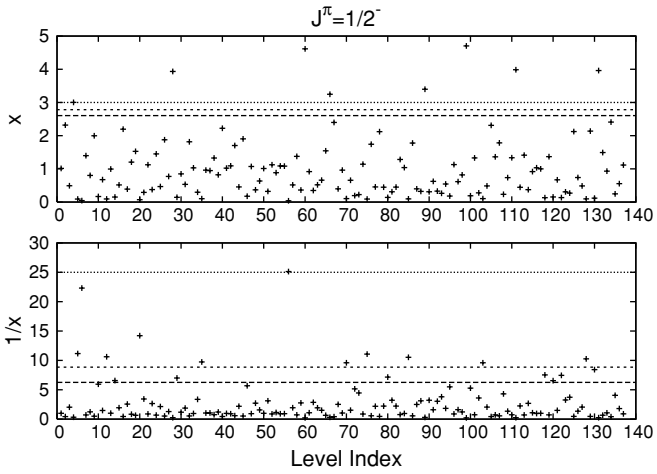

FIG. 4. Values of x and $1/x$ for states in this energy range previously assigned as $J^\pi = 1/2^-$. The dotted lines (from lowest to highest) represent the 2, 1, and 0.1% limits as discussed in the text.

and thus fewer levels are missed. In addition, fewer levels are misassigned because there is no ambiguity in J once ℓ is assigned. In general, for all of the statistical tests, the quality of the data (as measured by the number of missing levels and the number of spin misassignments) becomes worse with increasing ℓ and increasing J; the major reason for this is the greater difficulty in assigning J for the higher ℓ values.

Just as the Wigner distribution reflects the short-range anticorrelation of adjacent levels, the Δ_3 statistic measures long-range order. Results for the $1/2^+$ and $1/2^-$ levels are shown in Fig. 7. The agreement with the GOE prediction is reasonably good for the $1/2^+$ levels. The $1/2^-$ levels show significant deviations from the GOE prediction, while the other sequences are even worse. This is not surprising, since the effect of missing levels on Δ_3 is very pronounced: missing levels introduces a linear term which very quickly dominates the normal logarithmic term [25]. Thus one expects the sequence with the least ambiguity to show better agreement.

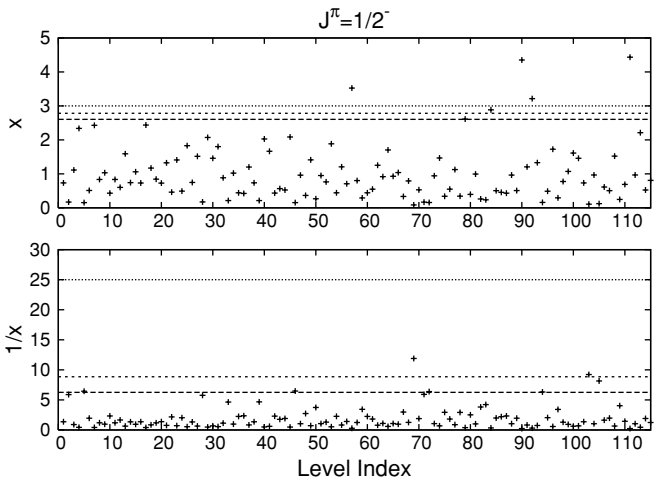

FIG. 5. Same as Fig. 4, but for states assigned $J^\pi = 1/2^-$ in the present work.

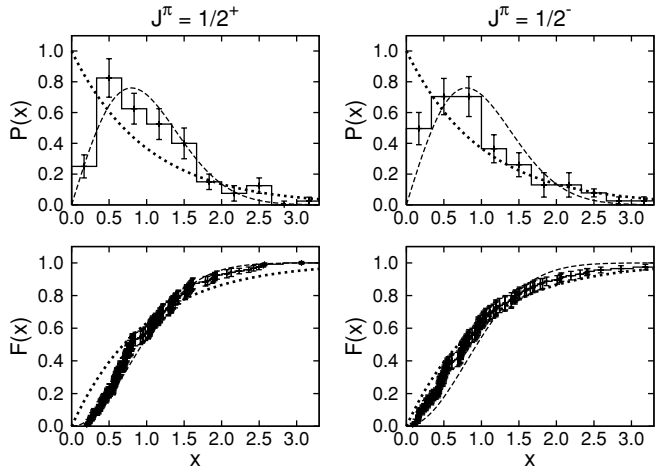

FIG. 6. Nearest-neighbor spacing distribution for $1/2^+$ and $1/2^-$ levels in $p + {}^{44}$Ca. Dashed line shows the Wigner distribution; the dotted line, the Poisson distribution.

The width distributions for these same two sequences are compared with the Porter-Thomas distribution in Fig. 8. The effects of missing small levels are clearly visible. All of the other sequences have width distributions that suggest an even larger fraction of missing levels.

Thus, based on these standard statistical tests, the $J = 1/2$ sequences are the best suited for detailed evaluation.

V. LEVEL DENSITIES AND STRENGTH FUNCTIONS

A. Missing level corrections

The discussion above suggests that many of the misassignments and missing levels have been corrected in the new data set. We are able to provide a quantitative estimate of the fraction of missing levels in a sequence. For the missing level problem, the standard approach assumes (1) that the underlying strength distribution is a Porter-Thomas (PT)

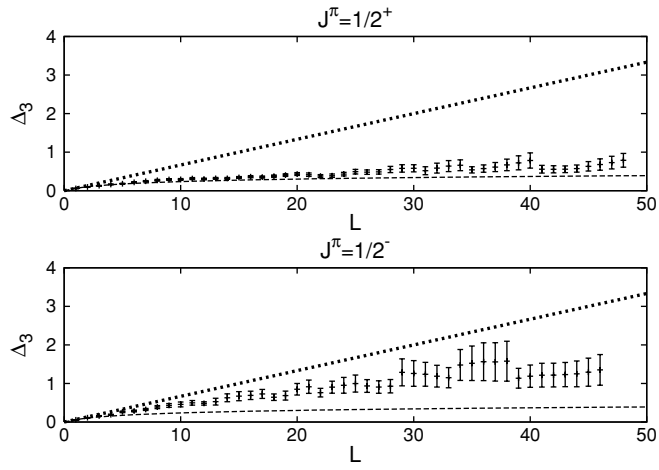

FIG. 7. Δ_3 for $1/2^+$ and $1/2^-$ levels in $p + {}^{44}$Ca. The dashed line shows the expectation for a GOE sequence; dotted line, the expectation for a Poisson sequence.

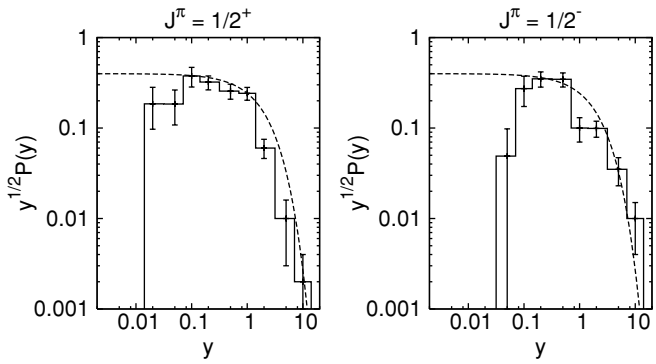

FIG. 8. Distribution of elastic scattering reduced widths for $1/2^+$ and $1/2^-$ levels in $p + {}^{44}$Ca. Dashed line shows the Porter-Thomas distribution.

distribution [24] and (2) that all of the levels with strengths below some threshold value are missed and that all of the levels with strengths above the cutoff value are observed. From the observed (incomplete) PT distribution, the fraction of missing levels is determined. This method works well as long as the behavior is purely statistical, but nonstatistical phenomena (e.g., doorway states) can have a major impact on the observed distribution and lead to an incorrect missing level correction. We have developed a method that uses the measured spacing distributions (for which the effects of nonstatistical phenomena are minimal) to determine the missing level correction [26,27]. In RMT, the spacings are independent of the widths and thus can provide an independent test for missing levels. Using the principle of maximum entropy, we obtained the probability distribution for imperfect eigenvalue sequences. (Recently, Bohigas and Pato [25] generalized our results.) We apply both correction methods to determine the missing fraction of levels in the $1/2^+$ and $1/2^-$ sequences.

1. Width correction method

The Gaussian assumption for the distribution of reduced width amplitudes leads to Eq. (11), the Porter-Thomas distribution. A modified Porter-Thomas distribution was introduced by Fröhner [28]:

$$P_F(y) = \begin{cases} 0 & : y < y_0 \\ \dfrac{1}{\mathrm{erfc}(\sqrt{y_0/2})} \dfrac{e^{-y/2}}{\sqrt{2\pi y}} & : y \geqslant y_0. \end{cases} \qquad (12)$$

The term involving the complementary error function ensures that the distribution is normalized to a total probability of 1. Maximizing the likelihood function constructed from the modified Porter-Thomas distribution yields the equation

$$\langle \gamma^2 \rangle = \langle \gamma^2 \rangle_{\mathrm{obs}} \left(1 + \sqrt{\frac{2y_0}{\pi}} \frac{e^{-y_0/2}}{\mathrm{erfc}\sqrt{y_0/2}} \right)^{-1}. \qquad (13)$$

The solution to this equation can be obtained iteratively as described in Ref. [27] and yields the most likely value for the average reduced width $\langle \gamma^2 \rangle$; that in turn can be used to determine the observed fraction of levels f.

2. Spacing correction method

The energies of nuclear resonances with the same quantum numbers form a GOE eigenvalue sequence. The nearest-neighbor spacings of perfect GOE sequences are to a good approximation described by the Wigner distribution [22] given in Eq. (1). To determine the observed fraction of levels from the experimental eigenvalues, we need the spacing distribution of an incomplete (imperfect) sequence. Because the positions of missing levels are random, the spacing distribution is affected by missing levels in a more complicated way than is the width distribution.

Some of the nearest-neighbor levels in the imperfect sequence are not actual nearest neighbors because of levels missing between the observed levels. Thus the nearest-neighbor spacing distribution for the imperfect sequence reflects the presence of higher-order spacing distributions. The observed nearest-neighbor spacing distribution (NNSD) for an imperfect sequence has been determined [27] to be

$$P(x) = \sum_{k=0}^{\infty} f(1-f)^k P(k;x), \qquad (14)$$

where $P(k;x)$ is the k-th nearest-neighbor spacing distribution. This result is general and therefore applies to any of the ensembles of RMT. To choose a particular ensemble requires specifying the appropriate $P(k;x)$ for that ensemble. We have applied both of these correction methods to the new $p + {}^{44}$Ca data set. The results are presented in the next section.

B. Level densities and strength functions

The results for the s-, p-, and d-wave sequences are summarized in Table III.

TABLE III. Summary of level density determinations for $\ell = 0$, $\ell = 1$, $\ell = 2$ states in $p + {}^{44}$Ca.

J^π	N_{obs}	f_{spacing}	f_{width}	f_{total}	N_{cor}	ρ (MeV^{-1})
$1/2^+$	121	$0.95^{+0.03}_{-0.04}$	$0.86^{+0.12}_{-0.10}$	$0.94^{+0.03}_{-0.04}$	128	127^{+7}_{-8}
$1/2^-$	116	0.87 ± 0.04	$0.83^{+0.13}_{-0.11}$	0.87 ± 0.04	134	132^{+8}_{-9}
$3/2^-$	178	0.85 ± 0.03	$0.66^{+0.08}_{-0.07}$	0.82 ± 0.03	216	215 ± 11
$3/2^+$	203	0.86 ± 0.03	$0.69^{+0.07}_{-0.06}$	0.83 ± 0.03	245	242 ± 12
$5/2^+$	117	0.85 ± 0.04	$0.76^{+0.10}_{-0.09}$	0.84 ± 0.04	140	138 ± 9

TABLE IV. Strength functions for $\ell = 0$, $\ell = 1$, $\ell = 2$ states in $p + {}^{44}$Ca

J^π	S (current work)	S (previous work)[a]
$1/2^+$	0.036 ± 0.005	0.045 ± 0.006
$1/2^-$	0.047 ± 0.007	0.049 ± 0.006
$3/2^-$	0.015 ± 0.002	0.019 ± 0.003
$3/2^+$	0.043 ± 0.004	0.047 ± 0.006
$5/2^+$	0.025 ± 0.003	0.035 ± 0.006

[a]Values taken from Ref. [26] and correspond to an energy range $E_p = 2.95$-3.72 MeV.

The corrected number of levels in a sequence is $N_{\rm cor} = N_{\rm obs}/f_{\rm total}$, where $f_{\rm total}$ is the fraction of levels observed (determined by combining the results of the two correction methods) for that sequence and $N_{\rm obs}$ is the number of observed levels in that sequence. The results for the two methods to determine the fraction of observed levels are in agreement for the two $J = 1/2$ sequences but do not agree as well for the higher spins. The uncertainties obtained with the spacing correction method are smaller than those obtained with the width correction method; this is common in our analyses but is not universally true. The level density is simply $\rho = N_{\rm cor}/\Delta E$, where ΔE is the energy interval studied.

The uncertainties in ρ arise from two sources, the statistical error due to the finite number of resonances in each sequence ($\Delta\rho_1$) and the statistical error due to the uncertainty in f ($\Delta\rho_2$). The two uncertainties have the form

$$\Delta\rho_1 = \rho\sqrt{\frac{0.27}{N_{\rm cor}}}, \qquad \Delta\rho_2 = \rho\frac{\Delta f}{f}, \tag{15}$$

where $\Delta\rho_1$ is taken from Lynn [29]. The two uncertainties are combined in quadrature to obtain the final $\Delta\rho$.

The level densities for these sequences are included in Table III; the two $J = 1/2$ values are in very good agreement with each other. For the $\ell = 2$ states, the greater difficulty in determining J means that misassigned levels are much more common; the values quoted here are less reliable for that reason but are listed for completeness.

We have also determined strength functions,

$$S = \langle\gamma^2\rangle/D, \tag{16}$$

for each sequence. These values are listed in Table IV and compared with results from previous resonance work [26] in ^{45}Sc. The new values tend to be slightly lower than but consistent with previous values. That behavior is consistent with the fact that the range of energies studied in this work is different from that in the previous study.

VI. SUMMARY AND CONCLUSIONS

A high resolution measurement of the ^{44}Ca(p, p_0) and ^{44}Ca(p, p_1) reactions was performed over the energy range $E_p = 2.50$–3.53 MeV. A total of 809 resonances were identified and analyzed. The purity and completeness of this ^{45}Sc resonance data set were tested with a variety of statistical tests that test short-range eigenvalue correlations, long-range eigenvalue correlations, and distributions of reduced widths. The $1/2^+$ levels are very pure and complete, while the $1/2^-$ data set appears to be of slightly lower quality. Other data sets are not as pure and complete due primarily to greater difficulties in uniquely identifying the spin of the levels.

The $J = 1/2$ resonances were used to examine whether nuclear level densities are parity dependent. The final results are $\rho(1/2^+) = 127^{+7}_{-8}$ MeV^{-1} and $\rho(1/2^-) = 132^{+8}_{-9}$ MeV^{-1}. Thus with what is arguably the most pure and complete set of proton resonance data ever obtained, there is no evidence of parity dependence of $J = 1/2$ levels at $E_x \approx 10$ MeV in ^{45}Sc.

ACKNOWLEDGMENTS

This work was supported in part by the U.S. Department of Energy under Grant Nos. DE-FG02-97-ER41042 and DE-FG02-96-ER40990. We thank W. C. Beal, D. B. McDevitt, and L. K. McLean for assistance with the data acquisition.

[1] A. Gilbert and A. G. W. Cameron, Can. J. Phys. **43**, 1446 (1965).
[2] W. Dilg, W. Schantl, H. Vonach, and M. Uhl, Nucl. Phys. **A217**, 269 (1973).
[3] A. S. Iljinov, M. V. Mebel, N. Bianchi, E. De Sanctis, C. Guaraldo, V. Lucherini, V. Muccifora, E. Polli, A. R. Reolon, and P. Rossi, Nucl. Phys. **A543**, 517 (1992).
[4] G. H. Lang, C. W. Johnson, S. E. Koonin, and W. E. Ormand, Phys. Rev. C **48**, 1518 (1993).
[5] H. Nakada and Y. Alhassid, Phys. Rev. Lett. **79**, 2939 (1997).
[6] H. Nakada and Y. Alhassid, Phys. Lett. **B436**, 231 (1998).
[7] S. I. Al-Quraishi, S. M. Grimes, T. N. Massey, and D. A. Resler, Phys. Rev. C **67**, 015803 (2003).
[8] U. Agvaanluvsan, G. E. Mitchell, J. F. Shriner, Jr., and M. Pato, Phys. Rev. C **67**, 064608 (2003).
[9] S. J. Lokitz, Ph.D. thesis, North Carolina State University, 2004.
[10] S. J. Lokitz, G. E. Mitchell, and J. F. Shriner, Jr., Phys. Lett. **B599**, 223 (2004).
[11] C. R. Westerfeldt, R. O. Nelson, E. G. Bilpuch, and G. E. Mitchell, Nucl. Instrum. Methods **A270**, 467 (1988).
[12] W. M. Wilson, E. G. Bilpuch, and G. E. Mitchell, Nucl. Phys. **A245**, 285 (1975).
[13] J. F. Shriner, Jr., E. G. Bilpuch, C. R. Westerfeldt, and G. E. Mitchell, Z. Phys. A **305**, 307 (1982).
[14] J. F. Shriner, Jr., K. M. Whatley, E. G. Bilpuch, C. R. Westerfeldt, and G. E. Mitchell, Z. Phys. A **313**, 51 (1983).
[15] B. W. Smith, Ph.D. thesis, Duke University, 1989.
[16] R. O. Nelson, E. G. Bilpuch, and G. E. Mitchell, Nucl. Instrum. Methods A **236**, 128 (1985).
[17] A. M. Lane and R. G. Thomas, Rev. Mod. Phys. **30**, 257 (1958).

[18] See EPAPS Document No. E-PRVCAN-71-419506 for ^{45}Sc resonance parameters. A direct link to this document may be found in the online article's HTML reference section. The document may also be reached via the EPAPS homepage (http://www.aip.org/pubservs/epaps.html) or from ftp.aip.org in the directory /epaps/. See the EPAPS homepage for more information.
[19] S. Åberg, A. Heine, G. E. Mitchell, and A. Richter, Phys. Lett. **B598**, 42 (2004).
[20] National Nuclear Data Center, Brookhaven National Laboratory.
[21] J. F. Shriner, Jr., E. G. Bilpuch, P. M. Endt, and G. E. Mitchell, Z. Phys. A **335**, 393 (1990).
[22] E. P. Wigner, in *Statistical Theories of Spectra: Fluctuations*, edited by C. E. Porter (Academic Press, New York, 1965), p. 199.
[23] F. J. Dyson and M. L. Mehta, J. Math. Phys. **4**, 701 (1963).
[24] C. E. Porter and R. G. Thomas, Phys. Rev. **104**, 483 (1956).
[25] O. Bohigas and M. P. Pato, Phys. Lett. **B595**, 171 (2004).
[26] U. Agvaanluvsan, Ph.D. thesis, North Carolina State University, 2002.
[27] U. Agvaanluvsan, G. E. Mitchell, J. F. Shriner, Jr., and M. Pato, Nucl. Instrum. Methods A **498**, 459 (2003).
[28] F. Fröhner, in *Nuclear Theory for Applications* (IAEA, Vienna, 1980), Vol. IAEA-SMR-43, p. 59.
[29] J. E. Lynn, *The Theory of Neutron Resonances* (Clarendon, Oxford, 1968).